Upconversion properties and dynamics study in Tm3+ and Yb3+ codoped CaSc2O4 oxide material

Jing Li, Jiahua Zhang, Zhendong Hao, Xia Zhang, Jihong Zhao, and Yongshi Luo

Citation: Journal of Applied Physics **113**, 223507 (2013); doi: 10.1063/1.4810898
View online: http://dx.doi.org/10.1063/1.4810898
View Table of Contents: http://scitation.aip.org/content/aip/journal/jap/113/22?ver=pdfcov
Published by the AIP Publishing

Upconversion properties and dynamics study in Tm^{3+} and Yb^{3+} codoped $CaSc_2O_4$ oxide material

Jing Li,[1,2] Jiahua Zhang,[1,a)] Zhendong Hao,[1] Xia Zhang,[1] Jihong Zhao,[3] and Yongshi Luo[1]
[1]*State Key Laboratory of Luminescence and Applications, Changchun Institute of Optics, Fine Mechanics and Physics, Chinese Academy of Sciences, 3888 Eastern South Lake Road, Changchun 130033, China*
[2]*Graduate School of Chinese Academy of Sciences, Beijing 100039, China*
[3]*Jilin Cancer Hospital, 1018 Huguang Road, Changchun 130012, China*

(Received 28 February 2013; accepted 28 May 2013; published online 12 June 2013)

The upconversion properties of Tm^{3+} and Yb^{3+} codoped $CaSc_2O_4$ phosphor excited at 980 nm are reported. The blue emission of Tm^{3+}:$^1G_4 \rightarrow {}^3H_6$, red emission of Tm^{3+}:$^1G_4 \rightarrow {}^3F_4$, near-infrared emissions of Tm^{3+}:$^3H_4 \rightarrow {}^3H_6$ (800 nm) and $^3F_4 \rightarrow {}^3H_6$ (1600 nm) are observed when excited Yb^{3+}:$^2F_{5/2}$ level. The spectral properties of Yb^{3+}:$^2F_{5/2}$ and Tm^{3+}:$^3F_4$, $^3H_4$, $^1G_4$ levels are described in detail as a function of Yb^{3+} and Tm^{3+} concentrations. By the trends of intensity ratios of Tm^{3+}:$^3F_4$ to Yb^{3+}:$^2F_{5/2}$ and Tm^{3+}:$^1G_4$ to $^3H_4$ with the doped concentrations, upconversion dynamics is analyzed in Tm^{3+} and Yb^{3+} codoped $CaSc_2O_4$ material. The concentration dependent lifetimes of Yb^{3+}:$^2F_{5/2}$ and Tm^{3+}:$^1G_4$, $^3H_4$ levels measured prove the existence of the efficient $Yb^{3+} \rightarrow Tm^{3+}$ energy transfer and followed $Tm^{3+} \rightarrow Yb^{3+}$ back-energy transfer processes, respectively. The energy transfer efficiency is up to 70% before concentration quenching occurrence. The back-energy transfer process is evidenced by the presence of the Yb^{3+}:$^2F_{5/2} \rightarrow {}^2F_{7/2}$ in the emission spectrum excited Tm^{3+}:$^1G_4$ level at 466 nm. The detailed spectroscopic study conduces to understand the upconversion dynamics process in Tm^{3+} and Yb^{3+} codoped excellent $CaSc_2O_4$ oxide material. © *2013 AIP Publishing LLC*.
[http://dx.doi.org/10.1063/1.4810898]

I. INTRODUCTION

The upconversion luminescence (UCL) properties of rare earth (RE) doped materials have been studied extensively over the past few decades because of the interesting physics research[1–3] as well as the potential applications in solid-state lasers, biological labeling, and infrared imaging.[4–6] The upconversion efficiency has been improved used fluorides as host materials due to the lower phonon frequency, but applications are restricted because of the poor chemical and thermal stability.[7,8] Oxide materials have high chemical durability and thermal stability which are significant for practical application. Some oxides also possess a relatively low phonon frequencies, which make it possible to obtain highly efficient UCL, such as silica-based,[4] bismuth-lead,[9] yttrium,[10] germanate[11] oxide materials. $CaSc_2O_4$ is a promising oxide host for achieving highly efficient up/down-conversion luminescence.[12–15] Tm^{3+} is an excellent RE ion for the very strong UCL around 800 nm where the biological tissue has the minimum absorption,[5,16] and considerably strong 480 nm (blue), 660 nm (red), and 360 nm (near-ultraviolet) UCL emissions.[10,11] The Tm^{3+} sensitized by Yb^{3+} is known as one of the most common combinations for efficient UCL. The upconversion characteristics of Tm^{3+} in Yb^{3+} sensitized crystals have been studied as early as 1970s.[1–3] Since then, the UCL properties of Tm^{3+} and Yb^{3+} ions have been reported in a range of host materials, such as glasses,[9,17,18] fluoride crystals,[19–22] and oxide materials.[4,23,24]

In our previous work, we demonstrated that doped concentration optimized $CaSc_2O_4$:Tm^{3+}, Yb^{3+} shows stronger UCL than doped concentration also optimized typical oxide upconverting phosphor Y_2O_3:Tm^{3+}, Yb^{3+} which has received great attention for exhibiting the efficient UCL under 980 nm excitation. The UCL enhancement is due to a large absorption cross section at 980 nm of Yb^{3+} and a large $Yb^{3+} \rightarrow Tm^{3+}$ first step energy transfer coefficient.[12] However, the UCL properties as a function of Tm^{3+} and Yb^{3+} concentrations in $CaSc_2O_4$:Tm^{3+}, Yb^{3+} have not been studied in detail yet.

The doped RE concentrations of materials usually play an important role in the UCL properties which must be optimized to achieve highly efficient luminescence.[18] Mita *et al.*[25] discovered energy transfer in oxide hosts have the stronger dependence on the doped concentrations than other hosts, such as fluorides. Recently, Etchart *et al.*[24] have reported the concentration dependent UCL properties of Tm^{3+} and Yb^{3+} codoped Y_2BaZnO_5 host. In the present work, we research doped concentration dependence of spectral distribution from 400 to 1750 nm and discuss the upconversion dynamics in Tm^{3+} and Yb^{3+} codoped $CaSc_2O_4$ material. The physical analysis of UCL process is carried out, by the trends of intensity ratios of Tm^{3+}:$^3F_4$ to Yb^{3+}:$^2F_{5/2}$ and Tm^{3+}:$^1G_4$ to $^3H_4$ with the doped concentrations. The experimental results are in good agreement with theoretical analysis. The results of concentration dependent lifetime measurement are exhibited. The highly efficient energy transfer from Yb^{3+} to Tm^{3+} is proved. The obvious back-energy transfers from Tm^{3+} to Yb^{3+} are observed.

a)Author to whom correspondence should be addressed. Electronic mail: zhangjh@ciomp.ac.cn. Tel./Fax: +86-431-8617-6317.

II. EXPERIMENTAL

A. Sample preparation

The series of samples investigated in this work with the general formula $CaSc_{2-y-x}O_4$:yTm^{3+}, xYb^{3+} ($1\% \le x \le 30\%$, $0.1\% \le y \le 2\%$) was prepared by a solid-state reaction.[15] The constituent carbonates or oxides $CaCO_3$ (99.9%), Sc_2O_3 (99.99%), Yb_2O_3 (99.99%), and Tm_2O_3 (99.99%) were employed as the raw materials, which were mixed homogeneously by an agate mortar for 30 min, placed in a crucible with a lid, then sintered at 1500 °C for 4 h.

B. Measurements and characterization

Powder X-ray diffraction (XRD) data were collected using Cu Kα radiation (λ = 1.54056 Å) on a Bruker D8 advance diffractometer equipped with a linear position-sensitive detector (PSD-50 m, M. Braun), operating at 40 kV and 40 mA with a step size of 0.01° (2θ) in the range of 15°–75°. The measurements of UCL emission spectra were performed by using a Triax 550 spectrometer (Jobin-Yvon) pumped with a power-controllable 980 nm diode laser. In fluorescence lifetime measurements, an optical parametric oscillator (OPO) was used as an excitation source, and the signals were detected by a Tektronix digital oscilloscope (TDS 3052). The emission spectrum under direct excitation was measured using a FLS920 spectrometer (Edinburgh Instruments, UK).

III. RESULTS AND DISCUSSION

The structures characterized by the XRD patterns are shown in Figure 1 for phosphors with the nominal compositions of $CaSc_2O_4$:$0.2\%Tm^{3+}$, xYb^{3+} (x = 5%, 10%, 20%, 30%). The pure phase $CaSc_2O_4$, in agreement with JCPDS card 20–0234, was synthesized without any impurity phase. The host lattice exhibits an orthorhombic $CaFe_2O_4$ structure with the space group *Pnam* (62). In this structure, Ca^{2+} is eightfold with the large effective ionic radius (1.12 Å) and Sc^{3+} sixfold with the small radius (0.745 Å).[26] The XRD peaks are observed to shift to smaller angles with increasing Yb^{3+} concentration, indicating that Yb^{3+} ions with larger ionic radius (0.868 Å) occupy Sc^{3+} (0.745 Å) sites in $CaSc_2O_4$ to expand the lattice cell volume. Yb^{3+} substitution for Sc^{3+} was also reported by Gaume *et al.* in Yb^{3+} singly doped $CaSc_2O_4$ sample.[27]

Figure 2 displays the UCL spectrum of $CaSc_2O_4$: $0.4\%Tm^{3+}$, $10\%Yb^{3+}$ under 980 nm excitation with output power density of 7 mW/mm^2. The strong emission bands centered around 480, 660, and 800 nm are attributed to the 4f-4f electronic transitions of Tm^{3+}:$^1G_4 \rightarrow {}^3H_6$, $^1G_4 \rightarrow {}^3F_4$, and $^3H_4 \rightarrow {}^3H_6$, respectively.[3] The emission band around 680–720 nm is ascribed to the Tm^{3+}:$^3F_{2,3} \rightarrow {}^3H_6$ transition.[20] The weaker emission around 530–565 nm is from $^5F_4 + {}^5S_2 \rightarrow {}^5I_8$ transition of trace impurity Ho^{3+} ions. It is confirmed by the UCL spectrum of $CaSc_2O_4$:Ho^{3+}, Yb^{3+} (supplemental material[28]). The RE elements are indeed chemically related; it is therefore difficult to separate them from each other thoroughly.[29]

In order to describe the population mechanism in Tm^{3+} and Yb^{3+} codoped $CaSc_2O_4$ material exactly, the dependence of spectral distribution on the Yb^{3+} and Tm^{3+} concentrations has been studied in detail. Figure 3 shows the infrared emission spectra from 1000 nm to 1750 nm of $CaSc_2O_4$:$0.2\%Tm^{3+}$, xYb^{3+} (x = 1%, 5%, 10%, 15%, 20%, 25%, 30%). Due to the strong self-quenching of Tm^{3+} ions,[3] the Tm^{3+} concentration is fixed at a low value of 0.2%. In the Tm^{3+} and Yb^{3+} codoped samples, 980 nm photon excites Yb^{3+}:$^2F_{7/2} \rightarrow {}^2F_{5/2}$ which exhibits fluorescence at 1000–1200 nm that excites Tm^{3+} ions into $^3H_5$ level through a nonresonant phonon-assisted energy transfer process. Tm^{3+} ions in $^3H_5$ level decay nonradiatively to $^3F_4$ level, then radiatively to the ground state emitting the photon around 1600 nm. The 1600 nm band detected corresponds to the higher energy side of Tm^{3+}:$^3F_4 \rightarrow {}^3H_4$ transition.[23,30] Its maximum emission is usually found around 1800 nm, which is out of the range of our study owing to the InGaAs detector used that has a cutoff wavelength of 1650 nm. The spectra in Figure 3 have been normalized as the maximum intensity of

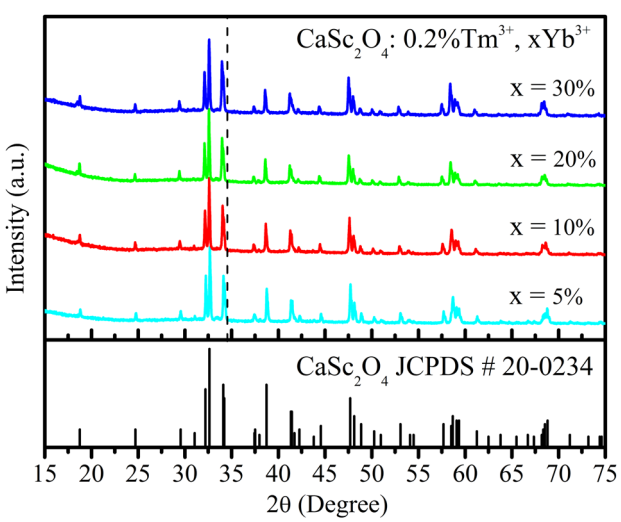

FIG. 1. XRD patterns for phosphors with the nominal compositions of $CaSc_2O_4$:$0.2\%Tm^{3+}$, xYb^{3+} (x = 5%, 10%, 20%, 30%).

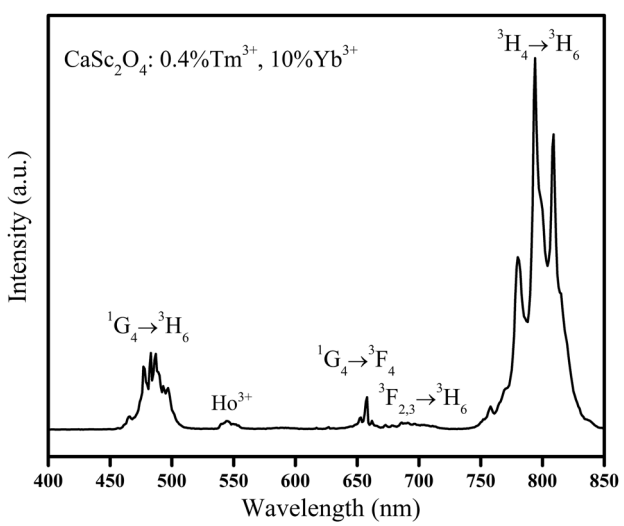

FIG. 2. UCL spectrum of $CaSc_2O_4$:$0.4\%Tm^{3+}$, $10\%Yb^{3+}$ under 980 nm excitation with a low pump density of 7 mW/mm^2.

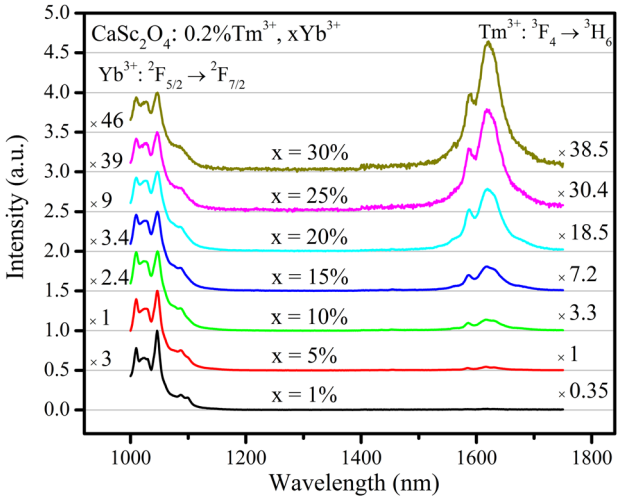

FIG. 3. Infrared spectra for $CaSc_2O_4$:0.2%Tm^{3+}, xYb^{3+} (x = 1%, 5%, 10%, 15%, 20%, 25%, 30%) under 980 nm excitation. Spectra are normalized to the maximum intensity of Yb^{3+} emission.

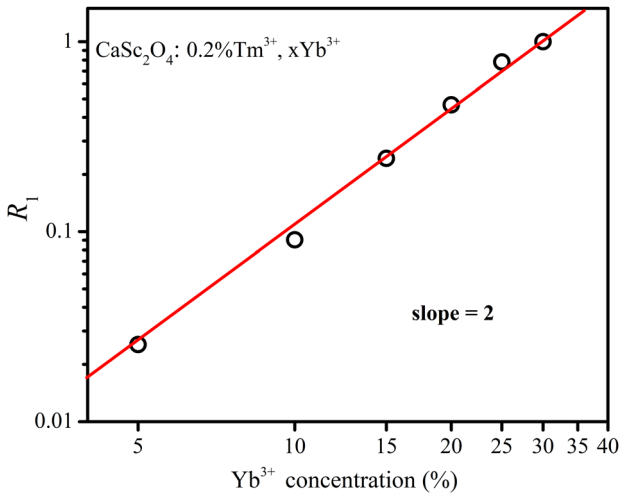

FIG. 4. Evolution of intensity ratio R_1 as a function of Yb^{3+} concentration.

Yb^{3+} emission. The left column value represents the enlargement factor of spectrum to the maximum. It shows Yb^{3+} emission reaches the maximum when Yb^{3+} concentration reaches to 5% then decreases quickly. The Tm^{3+}:$^3F_4 \rightarrow {}^3H_6$ emission around 1600 nm is enhanced by a factor shown on the right in comparison with that in doped 5%Yb^{3+} concentration sample. Combined the two column values, one can find that Tm^{3+}:$^3F_4$ emission gradually enhances when Yb^{3+} concentration increases from 1% to 15%, subsequently begins decreasing. The distances of Yb-Yb and Yb-Tm pairs decrease with Yb^{3+} concentration increasing, then the enhanced energy migration among Yb^{3+} ions speeds up energy transfer from Yb^{3+} to Tm^{3+}. It leads to the population of Yb^{3+}:$^2F_{5/2}$ level decrease. Due to the quenching of Tm^{3+} by Yb^{3+} ions,[3] the emission of Tm^{3+}:$^3F_4 \rightarrow {}^3H_6$ reaches a maximum, then drops down. The relative intensity of Tm^{3+} (1600 nm) to Yb^{3+} emission stands a rapid enhancement with Yb^{3+} concentration increasing. The x dependence of the intensity ratio (R_1) of Tm^{3+}:$^3F_4 \rightarrow {}^3H_6$ to Yb^{3+}:$^2F_{5/2} \rightarrow {}^2F_{7/2}$ obtained from emission spectra is plotted in a logarithmic diagram shown in Figure 4. The slope is found around 2, indicating R_1 is proportional to the square of Yb^{3+} concentration. Figure 5 shows the infrared emission spectra of $CaSc_2O_4$:yTm^{3+}, 10%Yb^{3+} (y = 0.1%, 0.2%, 0.4%, 0.6%, 1%, 1.4%, 2%). With Tm^{3+} concentration increasing, Yb^{3+} emission has a monotonic decline. It can be considered as the indication of efficient $Yb^{3+} \rightarrow Tm^{3+}$ energy transfer. The Tm^{3+} emission gradually increases as Tm^{3+} concentration increasing from 0.1% to 1%. As Tm^{3+} concentration over 1%, the intensity declines slightly as result of the self-absorption of Tm^{3+}.[31] Figure 6 illustrates a linear dependence of R_1 on the Tm^{3+} concentration.

Figure 7 shows the effect of Yb^{3+} (a) and Tm^{3+} (b) concentrations on the blue (480 nm) and near-infrared (800 nm) emissions. For fixed Tm^{3+} concentration at 0.2%, 480 nm and 800 nm emissions present the same trend with the Yb^{3+} concentration increasing. The optimized Yb^{3+} concentration is 10%. For fixed Yb^{3+} concentration at 10%, the strongest

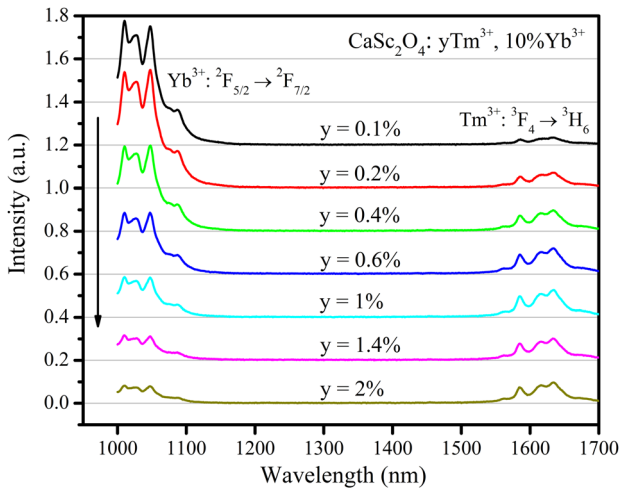

FIG. 5. Infrared spectra for $CaSc_2O_4$:yTm^{3+}, 10%Yb^{3+} (y = 0.1%, 0.2%, 0.4%, 0.6%, 1%, 1.4%, 2%) under 980 nm excitation.

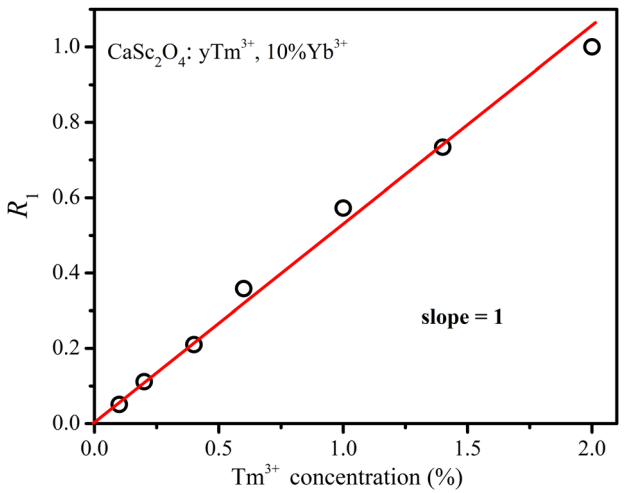

FIG. 6. Evolution of intensity ratio R_1 as a function of Tm^{3+} concentration.

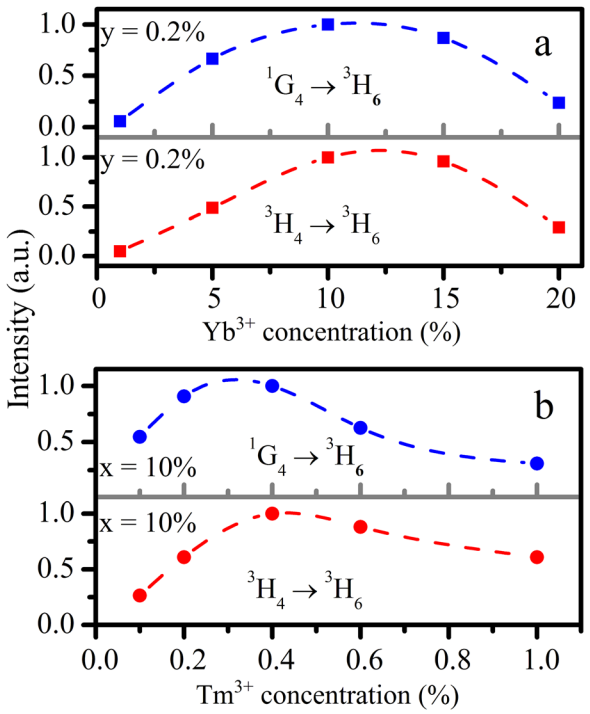

FIG. 7. Dependence of the blue ($^1G_4 \rightarrow {}^3H_6$) and near-infrared ($^3H_4 \rightarrow {}^3H_6$) UCL intensity on the concentration of Yb^{3+} (a) and Tm^{3+} (b) ions in $CaSc_2O_4$ material.

emissions are observed at Tm^{3+} concentration around 0.4%. When Tm^{3+} concentration exceeds 0.4%, 480 nm emission undergoes the faster descent compared with 800 nm. Figure 8 shows the evolutions of 480 nm to 800 nm intensity ratio (R_2) with the doped concentrations. In Figure 8(a), R_2 grows up until it reaches the maximum when x = 5%. Subsequently, it falls down. The value of R_2 decreases regularly as Tm^{3+} concentration increasing, as shown in Figure 8(b).

The pump power dependences of Yb^{3+}:$^2F_{5/2} \rightarrow {}^2F_{7/2}$ and Tm^{3+}:$^3F_4 \rightarrow {}^3H_6$, $^3H_4 \rightarrow {}^3H_6$, $^1G_4 \rightarrow {}^3H_6$ are measured under 980 nm excitation and plotted in a double logarithmic scales in Figure 9. The focus area of pumping beam was fixed about 80 mm^2. In the low pump power density, the slope n values for the four emissions are 1, 1, 2, and 3, respectively. It represents the number of pump step required to populate the corresponding emitting state. Due to

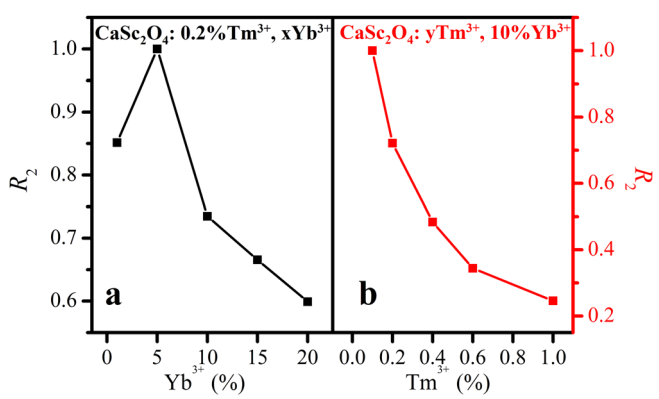

FIG. 8. Evolutions of intensity ratio R_2 as a function of Yb^{3+} (a) and Tm^{3+} (b) concentration.

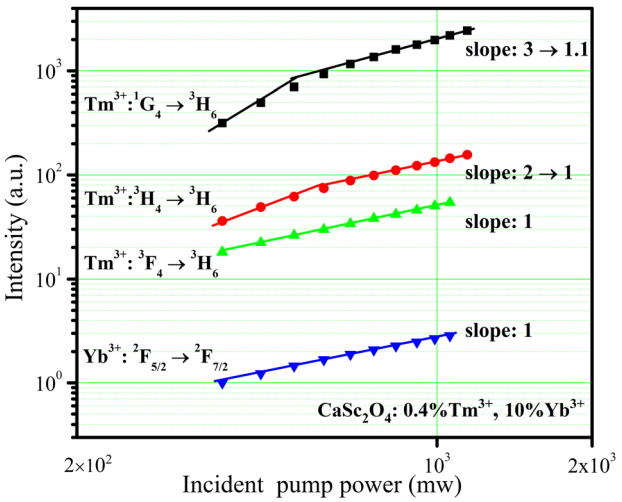

FIG. 9. Pump power dependences of emission intensities in $CaSc_2O_4$: 0.4%Tm^{3+}, 10%Yb^{3+} under a 980 nm excitation.

upconversion becomes dominant at the high pump power, all slopes gradually reduce to 1.[32] As the upconversion mechanism shown schematically in Figure 10, the energy transfer process is as follows:[3]

The first step:

$$Yb^{3+}:{}^2F_{5/2} + Tm^{3+}:{}^3H_6 \rightarrow Yb^{3+}:{}^2F_{7/2} + Tm^{3+}:{}^3H_5$$
$$Tm^{3+}:{}^3H_5 \rightarrow Tm^{3+}:{}^3F_4 \quad \text{multiphonon process}$$

The second step:

$$Yb^{3+}:{}^2F_{5/2} + Tm^{3+}:{}^3F_4 \rightarrow Yb^{3+}:{}^2F_{7/2} + Tm^{3+}:{}^3F_{2,3}$$
$$Tm^{3+}:{}^3F_{2,3} \rightarrow Tm^{3+}:{}^3H_4 \quad \text{multiphonon process}$$

The third step:

$$Yb^{3+}:{}^2F_{5/2} + Tm^{3+}:{}^3H_4 \rightarrow Yb^{3+}:{}^2F_{7/2} + Tm^{3+}:{}^1G_4$$

To verify and make a theoretical interpretation of UCL results mentioned above, we utilize the simplified steady-state equations

$$\frac{dn_0}{dt} = 0, \tag{1}$$

$$\frac{dn_1}{dt} = C_1 N_1 n_0 - \frac{n_1}{\tau_1} - C_2 N_1 n_1, \tag{2}$$

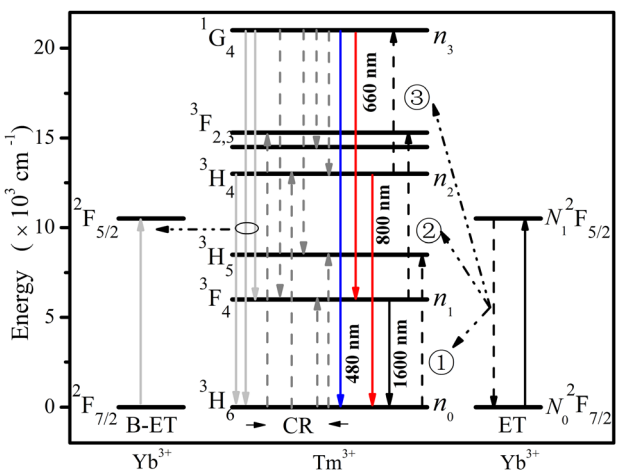

FIG. 10. Energy level diagrams and dominant upconversion mechanisms in $CaSc_2O_4$:Tm^{3+}, Yb^{3+} following 980 nm excitation.

$$\frac{dn_2}{dt} = C_2N_1n_1 - \frac{n_2}{\tau_2} - C_3N_1n_2, \quad (3)$$

$$\frac{dn_3}{dt} = C_3N_1n_2 - \frac{n_3}{\tau_3}, \quad (4)$$

$$\frac{dN_1}{dt} = \sigma IN_0 - C_1N_1n_0 - C_2N_1n_1 - C_3N_1n_2 - \frac{N_1}{\tau_{Yb}}, \quad (5)$$

where σ is the absorption cross section of Yb^{3+} ions, I is the incident pumping power, N_i is the population of i_{th} level of Yb^{3+}, n_i is the population of i_{th} level of Tm^{3+} involved in the upconversion process, τ_i is the measured lifetime of the i_{th} level of Tm^{3+} and τ_{Yb} is the measured lifetime of Yb^{3+}:$^2F_{5/2}$ level, C_i represents the coefficient for the i_{th} step energy transfer, and energy transfer rate W_i is the $W_i = C_in_{i-1}$.[33] The validity of this expression in our experiment will be discussed later.

A number of approximations have been made in our equations. The population of the intermediate states ($^3H_5$, $^3F_{2,3}$) is neglected due to the multiphonon decay fast to the lower levels. According to the faint emission of $^1G_4 \rightarrow {}^3F_4$ in Figure 3 (third step UCL), the population of Tm^{3+}:$^3F_4$ is mostly from the first step energy transfer. The equations neglect excitation from $^1G_4$ to higher Tm^{3+} levels by energy transfer due to the weak pump in our experiment.

According to Eqs. (1)–(5), we can derive a general physical description of intensity ratios R_1 and R_2

$$R_1 = \frac{\gamma_1 n_1}{\gamma_{Yb}N_1} = \frac{C_1\gamma_1 n_0}{\gamma_{Yb}\tau_1{}^{-1} + C_2\gamma_{Yb}N_1}, \quad (6)$$

$$R_2 = \frac{\gamma_3 n_3}{\gamma_2 n_2} = \frac{C_3\gamma_3 N_1\tau_3}{\gamma_2}, \quad (7)$$

where γ_i represents the radiative rate of i_{th} level of Tm^{3+} and γ_{Yb} is the radiative rate of Yb^{3+}:$^2F_{5/2}$ level, which are constant.

Figure 6 shows R_1 well satisfies a proportional relationship with the Tm^{3+} concentration (n_0). The τ_1 of Tm^{3+}:$^3F_4$ level is fixed due to a low up converted rate under weak pump.[3] On the basis of Eq. (6), C_1 is a constant. The result is consistent with theoretical premise, meaning the validity of theoretical analysis and experimental data. When n_0 is fixed, R_1 exhibits the quadratic dependence on Yb^{3+} concentration in Figure 4. The energy transfer rate W_1 can be simply written as $W_1 = C_1n_0(N_0)^2$. The observation may suggest the presence of three-body energy transfer process in Tm^{3+} and Yb^{3+} codoped $CaSc_2O_4$ samples.[34,35] As reported by Fong *et al.*,[34] many-body energy transfer process is important when the overlap between donor emission and acceptor absorption spectra is negligible. In Tm^{3+} and Yb^{3+} combination, the energy mismatch for the first step between Yb^{3+}:$^2F_{5/2}$ and Tm^{3+}:$^3H_5$ levels is 1650 cm^{-1},[3] while the cutoff phonon frequency of $CaSc_2O_4$ host lattice is only 540 cm^{-1}.[12] The ground state splitting of Yb^{3+} can reach 1008 cm^{-1} in $CaSc_2O_4$.[27] With the help of ground state Yb^{3+} ions, $Yb^{3+} \rightarrow Tm^{3+}$ energy transfer can be more effective. The three-body energy transfer of (Yb^{3+}:$^2F_{5/2}$-Yb^{3+}:$^2F_{7/2}$) $\rightarrow$ (Tm^{3+}:$^3H_6$-Tm^{3+}:$^3H_5$) + (Yb^{3+}:$^2F_{7/2(lowest)}$-Yb^{3+}:$^2F_{7/2(upper)}$)

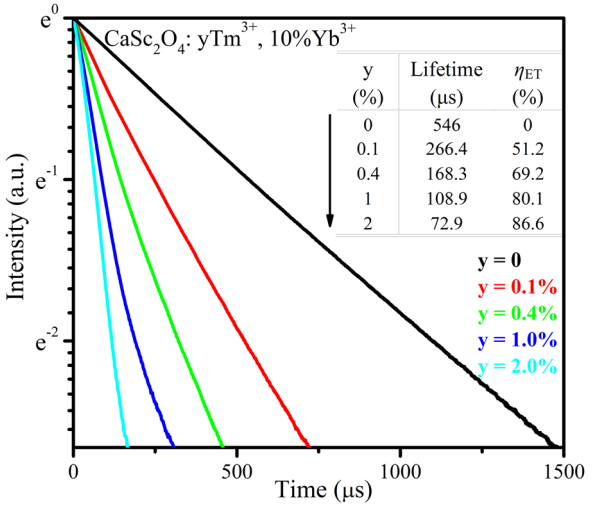

FIG. 11. Decay curves of Yb^{3+}:$^2F_{5/2} \rightarrow {}^2F_{7/2}$ in $CaSc_2O_4$:yTm^{3+}, 10%Yb^{3+} (y = 0%, 0.1%, 0.4%, 1%, 2%). Inset presents the calculated lifetime and energy transfer efficiency (η_{ET}) of sample with different Tm^{3+} concentration.

is easier to occur in samples with higher Yb^{3+} concentration.[34] This explanation requires evidence given by further study in the future.

Equation (7) exhibits R_2 is dependent on the N_1 and τ_3. For fixed Tm^{3+} concentration at 0.2%, N_1 and R_2 both reach the maximum when x = 5%, as shown in Figures 3 and 8(a). When Yb^{3+} concentration is unchanged, N_1 and R_2 decrease regularly with Tm^{3+} concentration increasing, as shown in Figures 5 and 8(b). It indicates N_1 is responsible for R_2. Furthermore, with Tm^{3+} concentration increasing, Tm-Tm distance decreases, leading to the strong cross relaxation (CR) of Tm^{3+} ions. The following four resonant ion-pair CR processes can result in the decline of intensity ratio R_2, displayed in Figure 10.

$^1G_4$ (Tm^{3+}) + $^3H_6$ (Tm^{3+}) $\rightarrow$ $^3H_4$ (Tm^{3+}) + $^3H_5$ (Tm^{3+}),[3,24]
$^1G_4$ (Tm^{3+}) + $^3H_6$ (Tm^{3+}) $\rightarrow$ $^3F_3$ (Tm^{3+}) + $^3F_4$ (Tm^{3+}),[3]
$^1G_4$ (Tm^{3+}) + $^3H_6$ (Tm^{3+}) $\rightarrow$ $^3H_5$ (Tm^{3+}) + $^3H_4$ (Tm^{3+}),[3,24]
$^1G_4$ (Tm^{3+}) + $^3H_6$ (Tm^{3+}) $\rightarrow$ $^3F_4$ (Tm^{3+}) + $^3F_2$ (Tm^{3+}).[3]

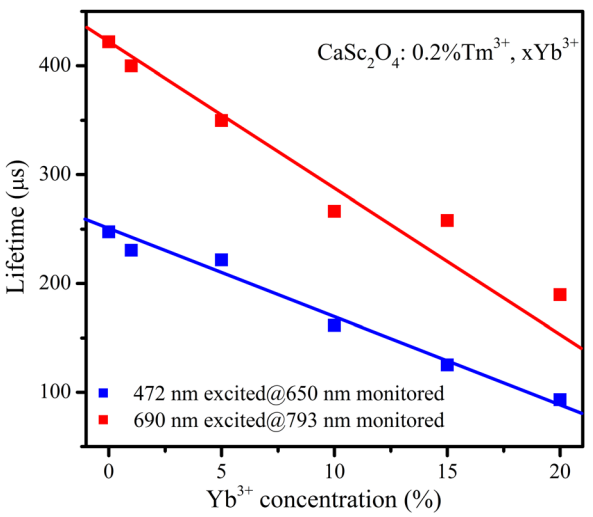

FIG. 12. Dependence of Tm^{3+}:$^3H_4$ and $^1G_4$ intrinsic lifetimes on Yb^{3+} concentration in $CaSc_2O_4$:0.2%Tm^{3+}, xYb^{3+} (x = 0%, 1%, 5%, 10%, 15%, 20%).

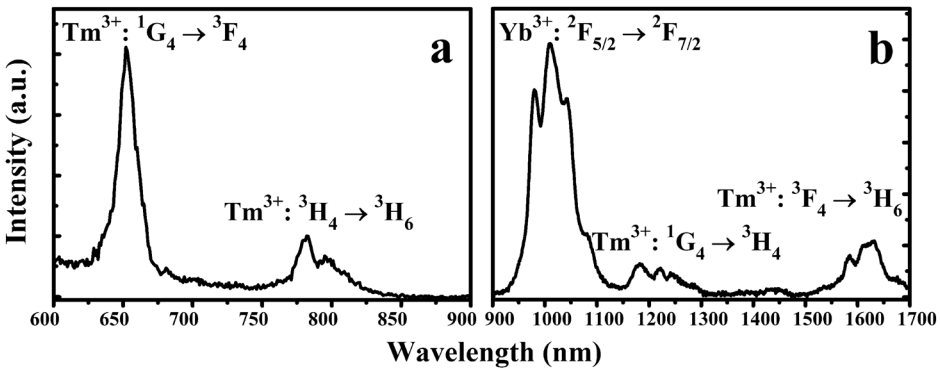

FIG. 13. Emission spectrum from 600 nm to 1700 nm of $CaSc_2O_4$:0.2%Tm^{3+}, 10%Yb^{3+} sample excited Tm^{3+}:$^1G_4$ level at 466 nm.

Figure 11 shows the decay curves of Yb^{3+}:$^2F_{5/2} \rightarrow {}^2F_{7/2}$ emission in $CaSc_2O_4$:yTm^{3+}, 10%Yb^{3+} (y = 0%, 0.1%, 0.4%, 1%, 2%). As Tm^{3+} concentration increasing, the decays rapidly speed up, confirming remarkable $Yb^{3+} \rightarrow Tm^{3+}$ energy transfer. The lifetime τ_{Yb0} and τ_{Yb} of Yb^{3+} in singly and doubly doped samples are calculated by integrating the area under the corresponding decay curves with the normalized initial intensity. The lifetime of Yb^{3+}:$^2F_{5/2}$ level decreases rapidly with Tm^{3+} concentration increasing as shown in Figure 11 (inset). The $Yb^{3+} \rightarrow Tm^{3+}$ energy transfer efficiency (η_{ET}) can be calculated by $\eta_{ET} = 1\text{-}\tau_{Yb}/\tau_{Yb0}$. For the concentration optimized sample with y = 0.4%, η_{ET} is up to 70%. Furthermore, decay curves of Yb^{3+} are all single-exponential, indicating a much faster energy migration among Yb^{3+} ions than $Yb^{3+} \rightarrow Tm^{3+}$ energy transfer. In this case, the $Yb^{3+} \rightarrow Tm^{3+}$ energy transfer rate always keeps at its initial decay rate, which is proportional to the acceptor concentration.[33] The energy transfer rate W_i is simply written as $W_i = C_i n_{i\text{-}1}$.

Figure 12 shows the Yb^{3+} concentration dependence of the intrinsic lifetimes of Tm^{3+}:$^3H_4$ and $^1G_4$ levels in $CaSc_2O_4$:0.2%Tm^{3+}, xYb^{3+} (x = 0%, 1%, 5%, 10%, 15%, 20%). The lifetimes of $^3H_4$ (τ_2) and $^1G_4$ (τ_3) levels both decrease quickly with increasing Yb^{3+} concentration. It indicates the existence of considerable back-energy transfer (B-ET) between Tm^{3+} and Yb^{3+} through cross pathways described by (Tm^{3+}:$^3H_4$, Yb^{3+}:$^2F_{7/2}$) → (Tm^{3+}:$^3H_6$, Yb^{3+}:$^2F_{5/2}$),[3,21] (Tm^{3+}:$^1G_4$, Yb^{3+}:$^2F_{7/2}$) → (Tm^{3+}:$^3H_5$, Yb^{3+}:$^2F_{5/2}$) or (Tm^{3+}:$^1G_4$, $2Yb^{3+}$:$^2F_{7/2}$) → (Tm^{3+}:$^3H_6$, $2Yb^{3+}$:$^2F_{5/2}$)[3] in Figure 10. The back-energy transfer efficiency ($\eta_{B\text{-}ET}$) can be calculated by $\eta_{B\text{-}ET} = 1\text{–}\tau_i/\tau_{i0}$ where τ_{i0} and τ_i is lifetime of Tm^{3+} in singly and doubly doped samples, respectively. The $\eta_{B\text{-}ET}$ of Tm^{3+}:$^3H_4$ and $^1G_4$ level is about 37% and 35% for sample with Yb^{3+} concentration at 10%, respectively. It can be seen that $\eta_{B\text{-}ET}$ from Tm^{3+} to Yb^{3+} is quite high and gradually increases with Yb^{3+} concentration increasing. Especially for Tm^{3+}:$^1G_4$ level, $\eta_{B\text{-}ET}$ is higher than the values in previous reports.[17,21] The emission spectrum from 600 nm to 1700 nm of $CaSc_2O_4$:0.2%Tm^{3+}, 10%Yb^{3+} excited at 466 nm corresponding to the absorption of Tm^{3+}:$^1G_4$ level is shown in Figure 13. Besides emissions of Tm^{3+}, Yb^{3+}:$^2F_{5/2} \rightarrow {}^2F_{7/2}$ emission has as well appeared, which proves the presence of B-ET from Tm^{3+}:$^1G_4$ to Yb^{3+}:$^2F_{5/2}$. Because of inevitable B-ET process for high Yb^{3+} concentration,[17] the optimized Yb^{3+} concentration for the 480 nm and 800 nm emissions (10%) is lower than that for 1600 nm (15%).

IV. CONCLUSION

Upconversion properties of Tm^{3+} and Yb^{3+} codoped $CaSc_2O_4$ oxide material in the visible and infrared regions have been investigated in detail. The efficient $Yb^{3+} \rightarrow Tm^{3+}$ energy transfer process is confirmed. The η_{ET} reaches up to 70% for the concentration optimized $CaSc_2O_4$:0.4%Tm^{3+}, 10%Yb^{3+} sample. The physical analysis of upconversion mechanism in $CaSc_2O_4$ system gets the following results:

(1) The intensity ratio R_1 satisfies a proportional relationship with the Tm^{3+} concentration. When Tm^{3+} concentration is fixed, R_1 exhibits the quadratic dependence on Yb^{3+} concentration. The first step energy transfer rate W_1 is written as $W_1 = C_1 n_0 (N_0)^2$. The observation indicates the presence of three-body energy transfer process among Tm^{3+} and Yb^{3+} ions in $CaSc_2O_4$ host.
(2) The intensity ratio R_2 exhibits the same trend with N_1. For fixed Tm^{3+} concentration, N_1 and R_2 reach the maximum at the same Yb^{3+} concentration (x = 5%). When Yb^{3+} concentration is unchanged, N_1 and R_2 decrease regularly with Tm^{3+} concentration increasing. It indicates N_1 is responsible for R_2. The CR processes occurred in Tm^{3+}:$^1G_4$ can further impact the intensity ratio R_2.
(3) The obvious back-energy transfer from Tm^{3+} to Yb^{3+} is proved in $CaSc_2O_4$ host by the Yb^{3+} concentration dependence of the intrinsic lifetimes of Tm^{3+}:$^3H_4$ and $^1G_4$ levels. The Yb^{3+}:$^2F_{5/2} \rightarrow {}^2F_{7/2}$ emission is also found when excited Tm^{3+}:$^1G_4$ level at 466 nm.

Our results reveal the UCL properties of $CaSc_2O_4$:Tm^{3+}, Yb^{3+} as a highly efficient and stable UCL oxide material for its diverse application. This will be of help in finding the new and efficient upconversion materials.

ACKNOWLEDGMENTS

This work was supported by the National Natural Science Foundation of China (10834006, 51172226, 61275055, 11274007, 11174278) and the Natural Science Foundation of Jilin province (201205024).

[1]R. A. Hewes and J. F. Sarver, Phys. Rev. **182**, 427 (1969).
[2]T. Miyakawa and D. L. Dexter, Phys. Rev. B **1**, 70 (1970).
[3]F. W. Ostermayer, Jr., J. P. van der Ziel, H. M. Marcos, L. G. Van Uitert, and J. E. Geusic, Phys. Rev. B **3**, 2698 (1971).

[4]D. A. Simpson, W. E. K. Gibbs, S. F. Collins, W. Blanc, B. Dussardier, G. Monnom, P. Peterka, and G. W. Baxter, Opt. Express **16**, 13781 (2008).
[5]M. Nyk, R. Kumar, T. Y. Ohulchanskyy, E. J. Bergey, and P. N. Prasad, Nano Lett. **8**, 3834 (2008).
[6]S. Schietinger, T. Aichele, H. Wang, T. Nann, and O. Benson, Nano Lett. **10**, 134 (2010).
[7]B. Dong, B. S. Cao, Y. Y. He, Z. Liu, Z. P. Li, and Z. Q. Feng, Adv. Mater. **24**, 1987 (2012).
[8]I. Etchart, A. Huignard, M. Bérard, M. N. Nordin, I. Hernández, R. J. Curry, W. P. Gillin, and A. K. Cheetham, J. Mater. Chem. **20**, 3989 (2010).
[9]Q. Y. Zhang, T. Li, Z. H. Jiang, X. H. Ji, and S. Buddhudu, Appl. Phys. Lett. **87**, 171911 (2005).
[10]X. R. Hou, S. M. Zhou, H. Lin, H. Teng, Y. K. Li, W. J. Li, and T. T. Jia, J. Appl. Phys. **107**, 083101 (2010).
[11]B. Zhou, L. L. Tao, W. Jin, and Y. H. Tsang, IEEE Photon. Technol. Lett. **24**, 1726 (2012).
[12]J. Li, J. H. Zhang, Z. D. Hao, X. Zhang, J. H. Zhao, and Y. S. Luo, Appl. Phys. Lett. **101**, 121905 (2012).
[13]Y. Shimomura, T. Kurushima, and N. Kijima, J. Electrochem. Soc. **154**, J234 (2007).
[14]Z. D. Hao, J. H. Zhang, X. Zhang, S. Z. Lu, and X. J. Wang, J. Electrochem. Soc. **156**, H193 (2009).
[15]Z. D. Hao, J. H. Zhang, X. Zhang, and X. J. Wang, Opt. Mater. **33**, 355 (2011).
[16]H. T. Wong, H. L. W. Chan, and J. H. Hao, Opt. Express **18**, 6123 (2010).
[17]B. Peng and T. Izumitani, Opt. Mater. **4**, 701 (1995).
[18]F. Lahoz, I. R. Martín, J. Méndez-Ramos, and P. Núñez, J. Chem. Phys. **120**, 6180 (2004).
[19]A. Braud, S. Girard, J. L. Doualan, M. Thuau, R. Moncorgé, and A. M. Tkachuk, Phys. Rev. B **61**, 5280 (2000).
[20]M. A. Noginov, M. Curley, P. Venkateswarlu, A. Williams, and H. P. Jenssen, J. Opt. Soc. Am. B **14**, 2126 (1997).
[21]X. X. Zhang, P. Hong, M. Bass, and B. H. T. Chai, Phys. Rev. B **51**, 9298 (1995).
[22]S. G. Xiao, X. L. Yang, J. W. Ding, and X. H. Yan, J. Phys. Chem. C **111**, 8161 (2007).
[23]F. Pandozzi, F. Vetrone, J. Boyer, R. Naccache, J. A. Capobianco, A. Speghini, and M. Bettinelli, J. Phys. Chem. B **109**, 17400 (2005).
[24]I. Etchart, I. Hernández, A. Huignard, M. Bérard, M. Laroche, W. P. Gillin, R. J. Curry, and A. K. Cheetham, J. Appl. Phys. **109**, 063104 (2011).
[25]Y. Mita, M. Togashi, Y. Umetsu, and H. Yamamoto, Jpn. J. Appl. Phys., Part 1 **40**, 5925 (2001).
[26]R. D. Shannon, Acta Crystallogr. **32**, 751 (1976).
[27]R. Gaume, B. Viana, J. Derouet, and D. Vivien, Opt. Mater. **22**, 107 (2003).
[28]See supplementary material at http://dx.doi.org/10.1063/1.4810898 for UCL spectrum of $CaSc_2O_4$:Ho^{3+}, Yb^{3+} by comparison with that of $CaSc_2O_4$:Tm^{3+}, Yb^{3+}.
[29]M. Ito, C. Goutaudier, Y. Guyot, K. Lebbou, T. Fukuda, and G. Boulon, J. Phys.: Condens. Matter **16**, 1501 (2004).
[30]Z. S. Xiao, R. Serna, F. Xu, and C. N. Afonso, Opt. Lett. **33**, 608 (2008).
[31]S. Guy, Phys. Rev. B **73**, 144101 (2006).
[32]J. F. Suyver, A. Aebischer, S. García-Revilla, P. Gerner, and H. U. Güdel, Phys. Rev. B **71**, 125123 (2005).
[33]M. M. Broer, D. L. Huber, W. M. Yen, and W. K. Zwicker, Phys. Rev. Lett. **49**, 394 (1982).
[34]F. K. Fong and D. J. Diestler, J. Chem. Phys. **56**, 2875 (1972).
[35]D. L. Andrews and R. D. Jenkins, J. Chem. Phys. **114**, 1089 (2001).